



## The Electrochemical Reactivity of 6.0 wt% Gd-Doped UO<sub>2</sub> in Aqueous Carbonate/Bicarbonate Solutions

Mayuri Razdan<sup>a,\*</sup> and David W. Shoesmith<sup>a,b,\*\*,z</sup>

<sup>a</sup>Department of Chemistry, Western University, London, Ontario N6A 5B7, Canada

<sup>b</sup>Surface Science Western, London, Ontario N6G 0J3, Canada

The effect of gadolinium doping on the anodic reactivity of UO<sub>2</sub> in aqueous carbonate solutions has been investigated voltammetrically, potentiostatically, by Raman spectroscopy and X-ray photoelectron spectroscopy. The mechanism of oxidation/dissolution is the same as on undoped UO<sub>2</sub> and lightly doped SIMFUEL (doped UO<sub>2</sub>) but the reactivity is significantly reduced. This is attributed to the formation of Gd<sup>III</sup>-Oxygen vacancy (O<sub>V</sub>) clusters which limits the availability of these vacancies required to accommodate excess O<sup>2-</sup> during matrix oxidation to U<sup>IV</sup><sub>1-2x</sub>U<sup>V</sup><sub>2x</sub>O<sub>2+x</sub>. The subsequent reaction of this oxidized surface layer to U<sup>VI</sup>O<sub>3</sub>·yH<sub>2</sub>O/U<sup>VI</sup>O<sub>2</sub>(CO<sub>3</sub>)<sub>x</sub><sup>(2-2x)+</sup> is also suppressed by Gd-doping. The overall oxidation/alteration (dissolution) reaction appears to be kinetically controlled by the creation of U<sup>VI</sup> surface species prior to dissolution.  
© 2014 The Electrochemical Society. [DOI: 10.1149/2.050404jes] All rights reserved.

Manuscript submitted December 30, 2013; revised manuscript received February 3, 2014. Published February 13, 2014. This was Paper 1801 presented at the San Francisco, California, Meeting of the Society, October 27–November 1, 2013.

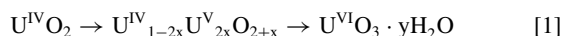
The direct disposal of spent nuclear fuel in geologic repositories has been under consideration internationally for over 30 years. In the Canadian concept, spent CANDU (CANada Deuterium Uranium) fuel bundles would be sealed in corrosion-resistant copper containers with an inner steel vessel and placed in an engineered repository constructed 500 m to 1000 m deep in a stable geologic location.<sup>1</sup> The concept is based on a multiple barrier system involving spent fuel bundles, the corrosion resistant container, and a clay buffer which seals the container within a deep geologic environment.<sup>2</sup> Container failure is not expected, since model calculations predict a loss of wall thickness by general corrosion of only a few microns.<sup>3</sup> However, it is judicious to assume some containers will fail allowing groundwater to contact the fuel causing radionuclide release.<sup>4</sup> Since the majority of the radionuclides in used fuel (spent UO<sub>2</sub>) are located within the oxide matrix, their release rate to the groundwater will be controlled by the fuel corrosion/dissolution rate.

Of key importance in determining fuel corrosion and, hence, radionuclide release rates, is the reactivity of the UO<sub>2</sub> matrix and how it is modified by in-reactor irradiation. The key changes expected to influence the reactivity of the fuel are; (i) the presence of non-stoichiometry, possibly associated with grain boundaries; (ii) the formation of noble metal particles which can act as microanodes or cathodes; and (iii) the rare earth (RE) doping of UO<sub>2</sub> which will change the conductivity and structural properties of the matrix.<sup>5</sup> We have been systematically studying all these influences. In this paper, the influence of trivalent rare earth doping (Gd<sup>III</sup> in this case) has been investigated.

The influence of fission products, including RE<sup>III</sup>, on the air oxidation of UO<sub>2</sub> has been well studied and reviewed.<sup>5-15</sup> These studies show that the oxidation of UO<sub>2</sub> (or UO<sub>2</sub> doped with low concentrations of impurities) proceeds through U<sub>3</sub>O<sub>7</sub> to the final product U<sub>3</sub>O<sub>8</sub>. By contrast UO<sub>2</sub> substantially doped (≥4 to 10%) with rare earths or other fission products proceeds via U<sub>4</sub>O<sub>9+y</sub> with this phase accommodating excess O<sup>2-</sup> beyond the nominal stoichiometry of UO<sub>2.25</sub>. The further conversion of U<sub>4</sub>O<sub>9+y</sub> to U<sub>3</sub>O<sub>8</sub> is also kinetically inhibited.

For Gd-doped UO<sub>2</sub>, the oxidized intermediate achieved the composition (U,Gd)O<sub>2.4</sub> which is more O-rich than U<sub>3</sub>O<sub>7</sub> (UO<sub>2.33</sub>). Similarly, spent LWR fuel with burn-ups in the range 190 to 960 MWh/kgU also yield U<sub>4</sub>O<sub>9+y</sub> with a stoichiometry of ~2.4 when oxidized at low temperature. By contrast, oxidation of spent CANDU fuel, which has a considerably lower burn up (120 to 320 MWh/kgU) and hence lower RE<sup>III</sup> doping, proceeded via a U<sub>3</sub>O<sub>7</sub> intermediate.<sup>6,8,15-17</sup>

We have shown<sup>18,19</sup> that the oxidation of UO<sub>2</sub> also occurs in a two step process,



with the first step involving the injection of O<sup>2-</sup> into vacant interstitial lattice sites to form a thin oxidized surface layer and the second step the conversion of the outer regions of this layer to a U<sup>VI</sup> alteration product layer. More recently, we have shown that the anodic reactivity of UO<sub>2</sub> is also suppressed by RE<sup>III</sup> (Gd, Dy) doping.<sup>20</sup> This reduced reactivity was attributed to the formation of RE<sup>III</sup>-O<sub>V</sub> (O<sub>V</sub> – oxygen vacancy) clusters accompanied by a contraction of the UO<sub>2</sub> lattice. This combination of features lead to a reduction in the availability of the O<sub>V</sub> required to accommodate the O<sup>2-</sup> incorporated during oxidation and a decreased mobility of O<sup>2-</sup> ions to deeper locations within the oxidized surface. This claim is consistent with the model calculations of Park and Olander<sup>21</sup> and the observations of Desgranges et al.<sup>22</sup>

Here, a more extensive electrochemical study of Gd-doped UO<sub>2</sub> (Gd-UO<sub>2</sub>), conducted in chloride solutions containing various concentrations of bicarbonate/carbonate (pH ~9) is described. Bicarbonate/carbonate is well known to complex UO<sub>2</sub><sup>2+</sup><sup>23</sup> and to accelerate UO<sub>2</sub> corrosion.<sup>5</sup> The anodic dissolution kinetics of UO<sub>2</sub> in carbonate solution have been previously studied.<sup>24</sup>

### Experimental

**Electrode material and preparation.**— All experiments were performed on chemically doped 6 wt% Gd-doped UO<sub>2</sub> (Gd-UO<sub>2</sub>) received from Cameco Corporation, Port Hope, Canada. Pellets were cut into disks (thickness ~3 mm) and fabricated into electrodes using a previously published methodology.<sup>19</sup> Before each experiment, the electrode was polished with wet SiC paper (1200 grit) and rinsed with Millipore water (ρ = 18.2M Ωcm). Subsequently the electrode was cleaned in an ultrasonic deionized water bath to remove any polishing residue. The electrode resistance, measured using electrochemical impedance spectroscopy, was ~50 Ω, which is very close to the value (~55 Ω) measured previously on doped UO<sub>2</sub> electrodes.<sup>19,25</sup>

All electrode preparation procedures were performed in an intermediate level radioactive laboratory. Cutting and polishing was performed in a dedicated fumehood within this laboratory, and the polishing and washing residues were disposed of using accepted procedures for the handling of low level radioactive wastes.

**Electrochemical cell and equipment.**— Experiments were performed in a standard three-electrode, three-compartment cell. A commercial saturated calomel reference electrode (SCE) (+0.242 V, 25°C vs. standard hydrogen electrode (SHE)) was used, and a Pt wire with a spot-welded Pt mesh (surface area ~6 cm<sup>2</sup>) was employed as the counter electrode. All potentials are quoted on the SCE scale. All electrochemical experiments were carried out using a Solartron model 1287 potentiostat to control applied potentials and record current responses. The current interrupt (IR) method was employed to compensate for the electrode resistance. Corware, version 3.0, software (Scribner Associates) was used to analyze the data.

\*Electrochemical Society Student Member.

\*\*Electrochemical Society Fellow.

<sup>z</sup>E-mail: dwshoesm@uwo.ca

**Solutions.**— Solutions were prepared with deionized water ( $\rho = 18.2 \text{ M}\Omega \text{ cm}$ ) purified using a Millipore milli-Q plus unit to remove organic and inorganic impurities. Carbonate ( $\text{Na}_2\text{CO}_3$ ) and bicarbonate ( $\text{NaHCO}_3$ ) (Caledon, >99%) were added to a  $0.1 \text{ mol.L}^{-1}$  sodium chloride ( $\text{NaCl}$ , Caledon >99%) solution to a total carbonate concentration  $[\text{HCO}_3^-/\text{CO}_3^{2-}] = 5 \times 10^{-2} \text{ mol.L}^{-1}$ . The pH was adjusted to the desired value of  $\sim 9.0$  using either dilute hydrochloric acid ( $\text{HCl}$ ) or sodium hydroxide ( $\text{NaOH}$ ) and was monitored with an Orion model 720A pH meter. All chemicals were of reagent grade. Prior to an experiment the solution in the cell was purged with Ar-gas (Praxair) for an hour and purging was then maintained throughout the experiment.

**Electrochemical techniques.**— In Cyclic Voltammetry (CV) experiments the potential ( $E$ ) was scanned from  $-1.5 \text{ V}$  to  $+0.4 \text{ V}$  and back while recording the current. In potentiostatic experiments a constant potential was applied to the electrode for an hour. Current-time profiles were recorded at potentials in the range from  $-0.5$  to  $+0.5 \text{ V}$ .

**Surface characterization.—Scanning electron microscopy (SEM)/energy dispersive X-ray (EDX) analysis.**— The surface morphology of the electrodes was determined using a field emission scanning electron microscope (Hitachi S-4500) equipped with a Quartz XOne energy dispersive X-ray analyzer. An electron beam with an accelerating voltage of  $15 \text{ kV}$  and a working distance of  $10 \text{ mm}$  was used to collect high resolution SEM micrographs at various magnifications ( $100\text{--}5000 \text{ X}$ ).

**X-ray photoelectron spectroscopy (XPS).**—X-ray photoelectron spectroscopy was used to investigate changes in stoichiometry of the electrode surface after electrochemical treatment at various applied potentials. A Kratos Axis Ultra spectrometer was used to record all spectra. An Al  $K_{\alpha}$  ( $15 \text{ mA}$ ,  $14 \text{ kV}$ ) high energy monochromatic X-ray radiation source ( $h\nu = 1486.6 \text{ eV}$ ) was used to bombard the fuel surface. The spectrometer work function was set to give a binding energy (BE) value of  $83.96 \text{ eV}$  for the metallic Au ( $4f_{7/2}$ ) line. Instrument dispersion was adjusted to give a BE of  $932.62 \text{ eV}$  for the metallic Cu  $2p_{3/2}$  line. Survey spectra were collected over the energy range from  $0$  to  $1100 \text{ eV}$  with an X-ray spot size  $\approx 300 \times 700 \mu\text{m}$  at a pass energy of  $160 \text{ eV}$ . High resolution spectra for all major species, i.e. U  $4f$ , O  $1s$ , C  $1s$  were recorded at a pass energy of  $20 \text{ eV}$  with a step size of  $0.05 \text{ eV}$ . Charge neutralization was used on all specimens. The C  $1s$  peak at  $285.0 \text{ eV}$  was used as a standard, when required, to correct for surface charging. All spectra were analyzed using CasaXPS software (version 2.3.14). The spectra were fitted using a 50% Gaussian/50% Lorentzian routine with a Shirley background correction.<sup>19</sup>

Quantification of U oxidation states ( $\text{U}^{\text{IV}}$ ,  $\text{U}^{\text{V}}$  and  $\text{U}^{\text{VI}}$ ) was achieved by curve-fitting the whole spectrum using the binding energies, as discussed elsewhere.<sup>26</sup> The resolved components in both spin-orbit split peaks and the associated satellite structures were used to calculate the total proportion of each oxidation state. The positions and shapes of the satellite structures were used to confirm the validity of the deconvolution of the U  $4f$  peaks.

On removal from the electrochemical cell, electrodes were gently rinsed with Millipore water and dried in an Ar-atmosphere (in an airtight sample container purged with Ar-gas) before transferring to the spectrometer.

**Raman spectroscopy.**—Raman spectra were obtained with a Renishaw 2000 Laser Raman spectrometer (Renishaw PLC., UK) equipped with a Leica DMLM microscope. Spectra were excited using a He-Ne laser with a wavelength of  $632.8 \text{ nm}$ . The laser beam was focused to  $\sim 2 \mu\text{m}$  diameter with a  $50\times$  uncoated objective lens on an electrode mounted on carbon tape attached to a glass slide. The power of the laser beam at the sample surface was kept at  $50\%$  to avoid laser heating effects. The calibration of the spectrometer was verified by acquiring spectra on a standard Si wafer which has only one intense Raman band ( $520 \text{ cm}^{-1}$ ). Spectra were measured for an exposure time of  $\sim 45 \text{ sec}$  over the wavenumber range  $120$  to  $1400 \text{ cm}^{-1}$ . Repeated measurements were carried out at different locations (plane area and pits/depressions) on the electrode to ensure that bands do

not show any shifts in vibrational frequencies or relative changes in peak intensities. The mixed Gaussian and Lorentzian peak model with a Shirley baseline correction used to fit the Raman spectra has been discussed elsewhere.<sup>19</sup>

## Results and Discussion

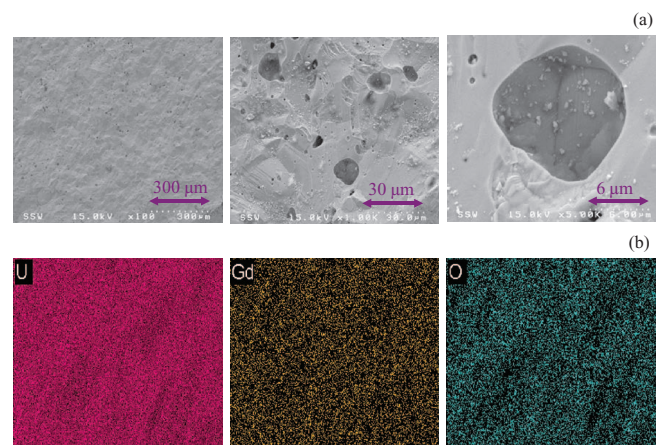
**Surface characterization.**— Figure 1a shows the typical surface morphology of the polished sintered Gd- $\text{UO}_2$  pellet at various magnifications revealing a plane surface with a small number of shallow voids but no other well defined features. EDX analysis (Fig. 1b) shows the Gd is evenly distributed within the  $\text{UO}_2$  matrix with no indication of a segregated Gd oxide. Such an even distribution is readily achieved since the ionic radii of  $\text{Gd}^{\text{III}}$  ( $\sim 0.107 \text{ nm}$ ) and  $\text{U}^{\text{IV}}$  ( $\sim 0.100 \text{ nm}$ ) are similar leading to a high solid solubility of  $\text{Gd}^{\text{III}}$  in the  $\text{U}^{\text{IV}}\text{O}_2$  matrix.

Figure 2a shows an optical image of the Gd- $\text{UO}_2$  electrode, and Fig. 2b the Raman spectra collected at the two numbered locations. Both spectra exhibited a band at  $450 \text{ cm}^{-1}$  which is assigned to the symmetric (O-U) stretching mode of the fluorite lattice of  $\text{UO}_2$ .<sup>27</sup> The broad, low intensity peak around  $1150 \text{ cm}^{-1}$  is commonly taken as diagnostic for the stoichiometric fluorite structure.<sup>28</sup>

The Raman spectrum obtained for Gd- $\text{UO}_2$  has been discussed in detail elsewhere.<sup>20</sup> Deconvolution of the  $500$  to  $700 \text{ cm}^{-1}$  region shows the dominant peak is at  $540 \text{ cm}^{-1}$ , which has been attributed to the presence of  $\text{Gd}^{\text{III}}\text{-O}_V$  clusters whose formation appeared to decrease the availability of the  $\text{O}_V$ s required to accommodate the O injected into the matrix during dissolution. The very shallow peak at  $640 \text{ cm}^{-1}$  provides supporting evidence that the lattice is effectively stoichiometric, this band having been attributed to the presence of cuboctahedral clusters associated with the presence of  $\text{U}_4\text{O}_9$ .<sup>29</sup>

The influence of Gd doping on the surface composition of  $\text{UO}_2$  was determined using XPS (Fig. 3). The fitted spectrum, which includes the  $\text{U}4f_{5/2}$ ,  $\text{U}4f_{7/2}$  and satellite peaks, clearly shows the presence of three U oxidation states (IV, V and VI). That  $\text{U}^{\text{IV}}$  is the dominant oxidation state present in the electrode surface is demonstrated by the sharpness of the spin-orbit peaks and from the location of the satellite peak at a binding energy  $\sim 7 \text{ eV}$  higher than the  $\text{U}4f_{5/2}$  peak. Identification of the satellite peaks is difficult since those associated with the  $\text{U}4f_{7/2}$  peak are generally obscured by the intense  $\text{U}4f_{5/2}$  peak or appear only as a shoulder. Besides,  $\text{U}^{\text{IV}}$ , a significant  $\text{U}^{\text{V}}$  content is observed. The presence of low amounts of  $\text{U}^{\text{VI}}$  may be due to slight air oxidation while transferring the electrode from the polishing area to the spectrometer.

**Voltammetry.**— Figure 4a shows a series of voltammograms recorded in solutions containing various carbonate concentrations ( $0$  to  $5 \times 10^{-2} \text{ mol.L}^{-1}$ ). The vertical dashed line shows that anodic oxidation becomes detectable in the forward scan for  $E \geq -0.2 \text{ V}$



**Figure 1.** (a) SEM micrographs, and (b) EDX maps recorded on a Gd- $\text{UO}_2$  electrode.

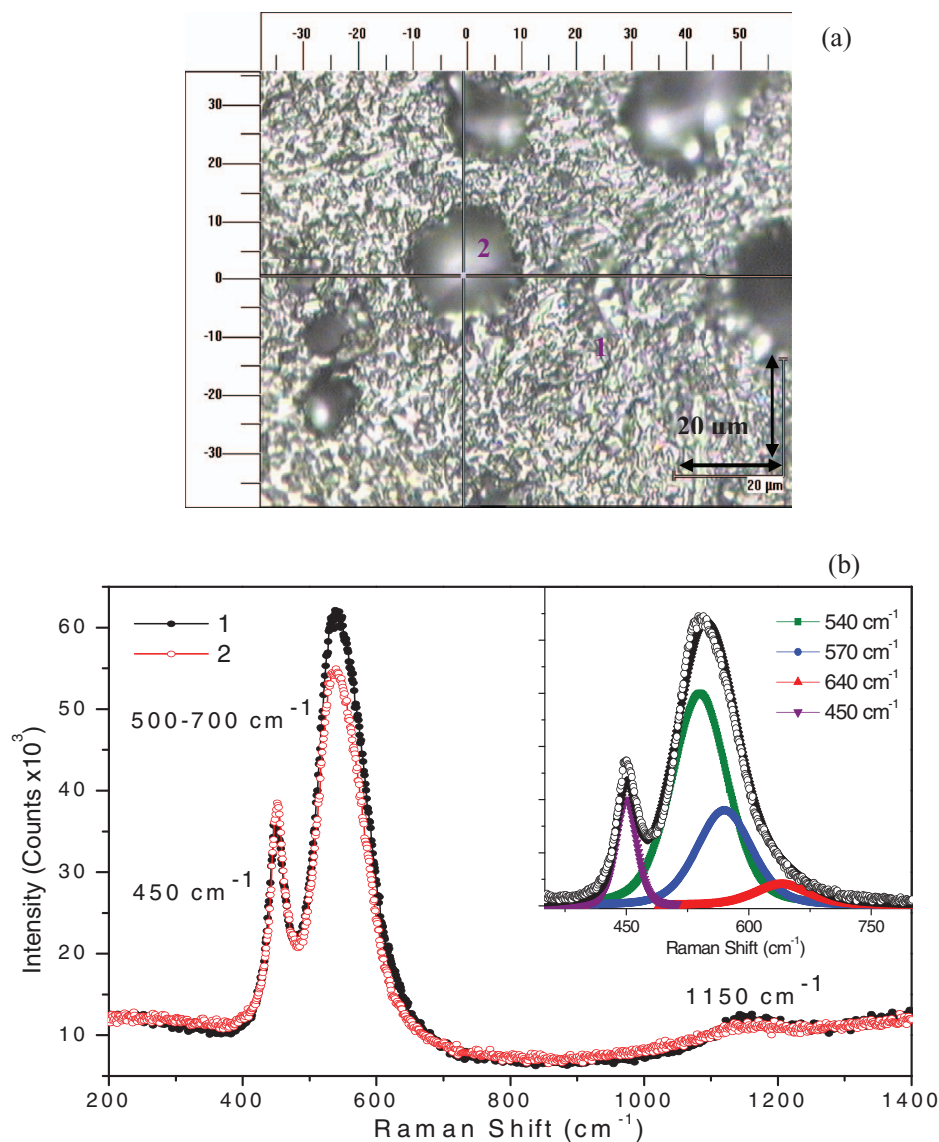


**Figure 2.** (a) An optical image of a polished Gd-UO<sub>2</sub> surface and, (b) the corresponding Raman spectra recorded at the two numbered locations.

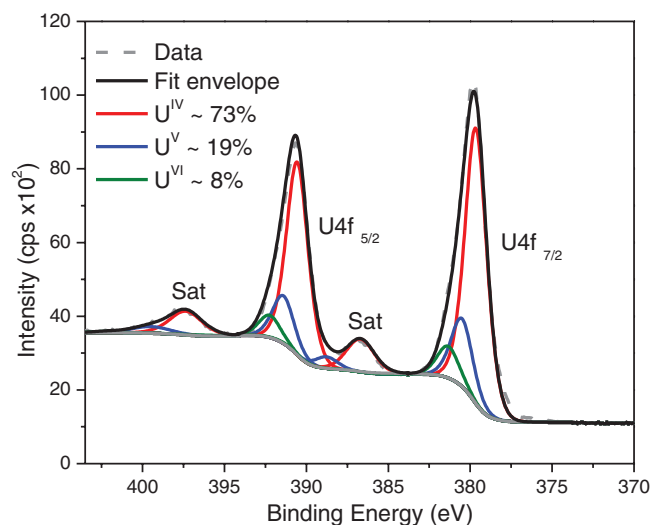


**Figure 3.** A fitted and background-corrected high resolution U4f XPS spectrum recorded on a polished Gd-UO<sub>2</sub> electrode.

with and without carbonate in solution. As discussed elsewhere for SIMFUEL<sup>19</sup> and Gd-doped UO<sub>2</sub>,<sup>20</sup> this can be attributed to the oxidation of a thin surface layer to a mixed U<sup>IV</sup>/U<sup>V</sup> oxide (U<sup>IV</sup><sub>1-2x</sub>U<sup>V</sup><sub>2x</sub>O<sub>2+x</sub>). Over the carbonate concentration range from 0 to  $5 \times 10^{-4}$  mol.L<sup>-1</sup>, a current plateau is observed around 0 to 0.2 V, while at more positive potentials the current increases substantially but is independent of carbonate concentration. For carbonate concentrations in the range  $10^{-3}$  to  $10^{-2}$  mol.L<sup>-1</sup>, the current in this plateau region increases markedly, but the current at the anodic limit of 0.4 V is suppressed. A further increase in carbonate concentration to  $5 \times 10^{-2}$  mol.L<sup>-1</sup> leads to almost no current increase up to  $\sim -0.2$  V, the disappearance of the plateau, and a marked increase in current at the anodic limit of 0.4 V.

On the reverse scan, a broad cathodic reduction peak occurs with a maximum at  $\sim -0.75$  V. The size and breadth of this peak is independent of carbonate concentration. This reduction peak is generally associated with the reduction of a U<sup>IV</sup><sub>1-2x</sub>U<sup>V</sup><sub>2x</sub>O<sub>2+x</sub>/UO<sub>3</sub>.yH<sub>2</sub>O surface layer in the absence of carbonate<sup>20</sup> and on 1.5 at% SIMFUEL is considerably reduced in size when carbonate is present. The disappearance of this reduction peak on SIMFUEL was attributed to the enhanced dissolution of U<sup>VI</sup> (as U<sup>VI</sup>O<sub>2</sub>(CO<sub>3</sub>)<sub>x</sub><sup>(2-2x)+</sup>) on the forward scan.<sup>30</sup>

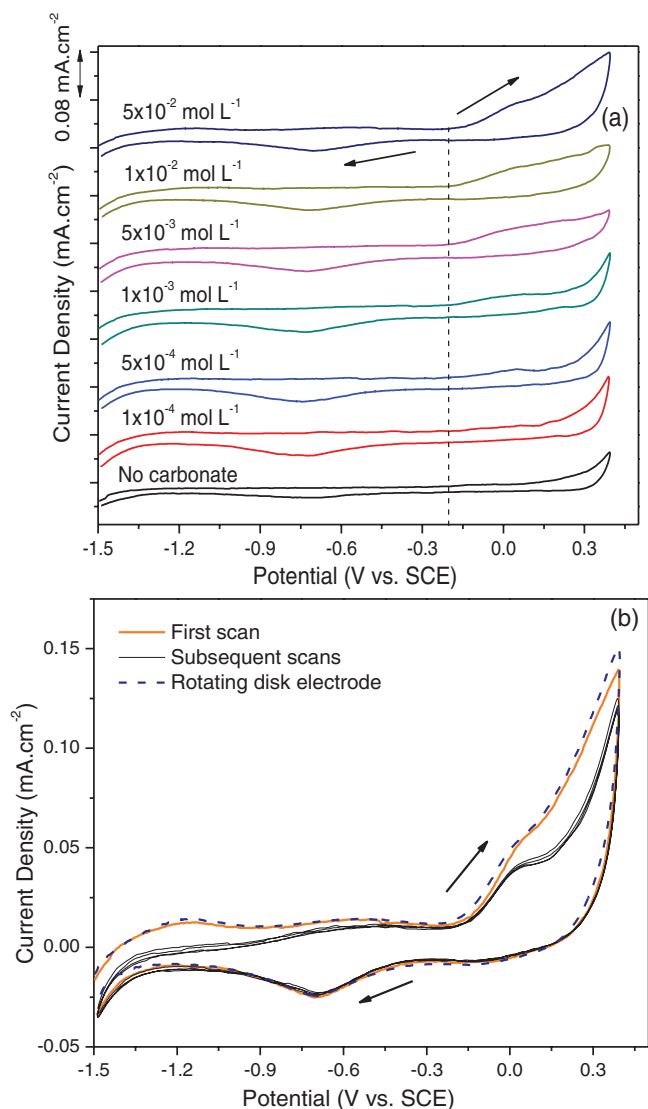


**Figure 4.** CVs recorded on a freshly polished Gd- $\text{UO}_2$  electrode in an Ar-purged  $0.1 \text{ mol.L}^{-1}$  NaCl, pH 9 solution: (a)  $[\text{HCO}_3^-/\text{CO}_3^{2-}] = 0$  to  $5 \times 10^{-2} \text{ mol.L}^{-1}$  (b) Repeated scans in a solution containing  $[\text{HCO}_3^-/\text{CO}_3^{2-}] = 5 \times 10^{-2} \text{ mol.L}^{-1}$  and on a rotating disk electrode at 16.67 Hz.

The presence of this reduction peak in Fig. 4a indicates that an oxidized surface layer is maintained on the Gd- $\text{UO}_2$  surface despite the presence of carbonate. Although only shallow, and difficult to see on the scale of this figure, a second shallow reduction peak (more visible in Fig. 4b) is observed in the potential range  $+0.1 \text{ V}$  to  $-0.2 \text{ V}$ . This peak is only observed at high carbonate concentration suggesting it could be due to the presence of a thin layer of readily reducible  $\text{U}^{\text{VI}}\text{O}_2\text{CO}_3$ .

Figure 4b shows there is a significant difference in the anodic current observed on the first scan compared to subsequent scans (recorded without repolishing the electrode). This may reflect the slightly enhanced anodic oxidation of the electrode surface due to the polishing procedure. Once this effect of polishing damage is removed the subsequent scans show very reproducible behavior including a measurable anodic reactivity between  $-0.9 \text{ V}$  and  $-0.2 \text{ V}$ . Previously, oxidation in this potential region has been associated with the presence of readily oxidizable non-stoichiometric  $\text{UO}_{2+x}$  locations on the electrode surface, possibly associated with grain boundaries.<sup>4</sup> The lack of any influence of electrode rotation on both the anodic and cathodic currents demonstrates that the anodic and cathodic processes involved

are activation or chemically controlled and not influenced by solution diffusion processes.

**Potentiostatic oxidation.**— Figure 5 shows a series of current density ( $\log i$ ) vs. time ( $\log t$ ) plots recorded at individual potentials in the range  $-0.5$  to  $0.5 \text{ V}$  in  $0.1 \text{ mol.L}^{-1}$  NaCl without ((a), (c), (e)) and with ((b), (d), (f)) carbonate ( $5 \times 10^{-2} \text{ mol.L}^{-1}$ ) present.

Although not shown in Fig. 5b, for the carbonate solution, at the lowest potential employed,  $-0.5 \text{ V}$ , the current rapidly became cathodic (Fig. 5b black solid line) and eventually established a value in the range  $1\text{--}3 \mu\text{A}$ . A similar cathodic current was not observed at this potential in the non-carbonate containing solution, Fig. 5a. Although not shown in Fig. 5b (since the currents become extremely noisy), for all potentials  $\leq 0 \text{ V}$  in the carbonate solution, the final current recorded is negative. The absence of a similar shift to negative currents for potentials in this range in the absence of carbonate suggests this cathodic current may be attributable to reduction of protons provided by bicarbonate dissociation. Over the potential range  $-0.4$  to  $-0.1 \text{ V}$  (Fig. 5a, 5b), the anodic current decreased with time with only a slight dependence on potential, consistent with a loss in surface reactivity. The current stabilizes in the long term beyond 1000 s in solutions both with and without carbonate. Although the  $\log i$ - $\log t$  plots have the same slopes at each potential in the respective solutions, the current densities in the carbonate solution are significantly higher.

At short times ( $\leq 100\text{s}$ ) in the potential range  $0$  to  $0.3 \text{ V}$  in the absence of carbonate, the  $\log i$  -  $\log t$  plots, (Fig. 5c), are linear indicating a loss of surface reactivity with time. As observed in the CVs the current is only slightly dependent on potential until the potential exceeds  $\sim 0.25 \text{ V}$ . At long times ( $> 1000\text{s}$ ), the current increases markedly and tends toward a steady-state value for potentials  $> 0.3 \text{ V}$ , Fig. 5e. This increase in current at longer times was shown to be due to local acidification within surface asperities due to the hydrolysis of dissolved  $\text{UO}_2^{2+}$

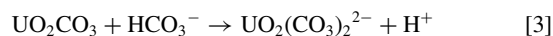


which leads to accelerated anodic dissolution at these locations.

In carbonate-containing solutions similar behavior is observed at short times (Fig. 5d) in the potential range  $0$  to  $0.3 \text{ V}$  indicating a similar surface deactivating film formation process. Except at the most positive potentials ( $\geq 0.4 \text{ V}$ ; (Fig. 5f)) the current in this time interval is higher than in the absence of carbonate suggesting an enhanced anodic dissolution process.

The major difference in behavior when carbonate is present occurs at longer times for potentials  $\geq 0 \text{ V}$ . Over the range  $0 \text{ V}$  to  $0.30 \text{ V}$  (Fig. 5c, 5d) the current in carbonate containing solutions is considerably higher suggesting, as expected, an enhanced anodic dissolution (as  $\text{U}^{\text{VI}}\text{O}_2(\text{CO}_3)_x^{(2-2x)+}$ ). At the highest potentials the current is lower than in the absence of carbonate (Fig. 5e and 5f). This can be attributed to buffering of the local surface pH and the avoidance of accelerated dissolution due to local acidification.

Figure 6 shows the final steady state anodic current ( $i_{\text{ss}}$ ) values recorded after 1 hour of polarization plotted against  $E$  in the Tafel format ( $\log i_{\text{ss}}$  vs  $E$ ). A similar set of data previously obtained for 1.5 at% SIMFUEL in the presence of carbonate is included.<sup>30</sup> In the presence of carbonate, the anodic currents for Gd- $\text{UO}_2$  are considerably lower than those recorded on SIMFUEL. The Tafel slopes at lower potentials ( $\leq 0.3 \text{ V}$ ) are in the range  $120$  to  $150 \text{ mV}$  indicating the mechanism of anodic oxidation/dissolution does not change, only the overall reactivity of the matrix. At higher potentials the currents tend to a plateau value although this occurs at lower potentials on the Gd- $\text{UO}_2$  electrode than on the SIMFUEL. The observation of a potential-independent current on SIMFUEL at positive potentials was previously attributed to control of the overall anodic dissolution process by the chemical dissolution of a  $\text{UO}_2\text{CO}_3$  surface layer



In the absence of carbonate, the Tafel slope at low potentials ( $100\text{--}300 \text{ mV}$ ) is very low ( $412 \text{ mV}$ ) indicating the formation of an almost

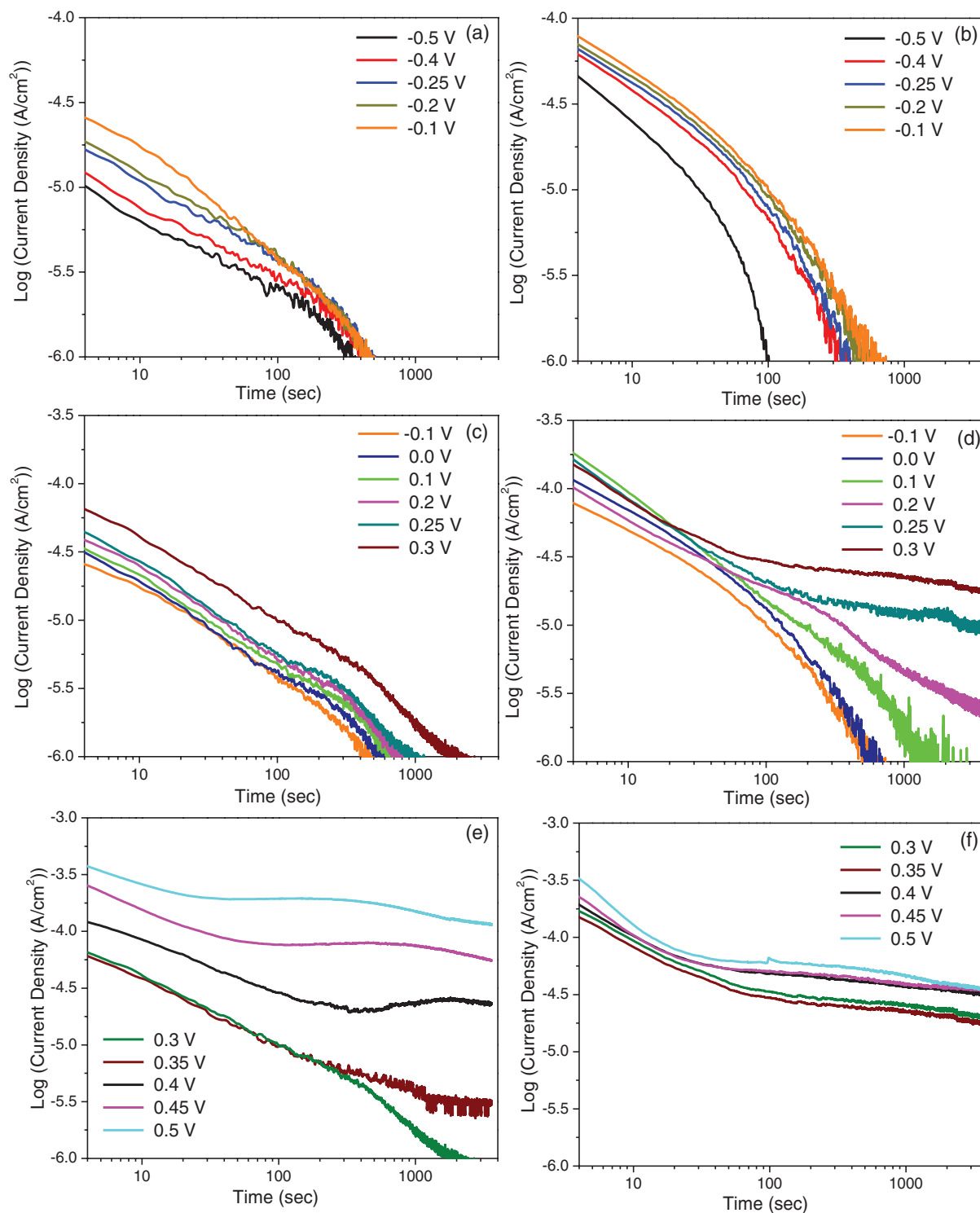


**Figure 5.** Potentiostatic current-time curves recorded for 1 h in Ar-purged 0.1 mol.L<sup>-1</sup> NaCl, pH 9, in the potential range  $-0.5$  to  $0.5$  V without (a, c, e) and with (b, d, f) carbonate ( $[\text{HCO}_3^-/\text{CO}_3^{2-}] = 5 \times 10^{-2}$  mol.L<sup>-1</sup>). The current recorded at  $-0.5$  V in carbonate solution (b) switched from anodic to cathodic current after 100 s. The final currents established at all potentials  $\leq 0$  V were also negative but this is not shown for clarity.

passivating surface layer. The influence of local acidification leading to a higher current at more positive potentials ( $>0.3$  V) is clear in Fig. 6.

**XPS analysis.**— A detailed investigation of the oxidation state of U in the surface of an anodically oxidized Gd-UO<sub>2</sub> electrode was carried out using XPS. Figures 7 and 8 show representative deconvoluted

spectra for the U ( $4f_{5/2}$ ) and U ( $4f_{7/2}$ ) regions and their associated satellite structures recorded after a 1 hr of potentiostatic polarization at  $-0.5$ ,  $-0.1$ ,  $0.2$  and  $0.5$  V in solutions without and with carbonate, respectively. The vertical dashed lines indicate the positions of the satellite peaks expected for U<sup>IV</sup> ( $-0.5$  and  $-0.1$  V), U<sup>V</sup> ( $-0.1$ ,  $0.2$  and  $0.5$  V), and (hidden) for U<sup>VI</sup> ( $0.2$  and  $0.5$  V) used to confirm the deconvolution of the main peaks. The percentages of U<sup>IV</sup>, U<sup>V</sup> and U<sup>VI</sup>

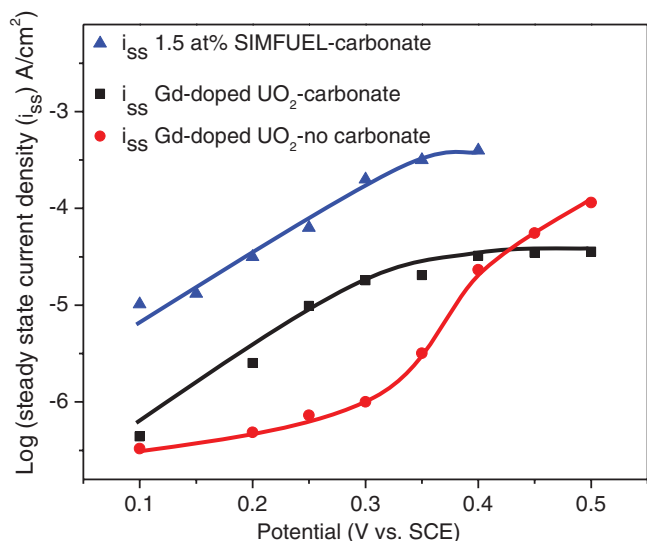


**Figure 6.** Tafel plots for the anodic oxidation/dissolution of a Gd-doped  $\text{UO}_2$  electrode in an Ar-purged  $0.1 \text{ mol.L}^{-1}$  NaCl solution, pH 9, with  $([\text{HCO}_3^-/\text{CO}_3^{2-}] = 5 \times 10^{-2} \text{ mol.L}^{-1})$  and without carbonate. Data recorded on a 1.5 at% SIMFUEL in the carbonate solution is also included.<sup>30</sup>

in the electrode surface are shown as a function of applied potential in Fig. 9.

In the potential range  $-0.5$  to  $-0.25$  V, changes in the composition of the surface are undetectable indicating that a potential of  $\sim -0.25$  V is the lower limit for surface oxidation. The traces of  $\text{U}^{\text{VI}}$  detected in this range may be due to a slight degree of surface oxidation on transfer of the electrode from the electrochemical cell to the vacuum chamber of the spectrometer. The measurable fraction of  $\text{U}^{\text{V}}$  is likely due to the  $\text{RE}^{\text{III}}$  doping of the electrode. This leaves unexplained the small degree of anodic oxidation observed electrochemically in this potential range (Fig. 4, Fig. 5a, 5b), which leads to a loss of reactivity of the surface.

Over the potential range  $-0.2$  to  $0.1$  V, anodic oxidation is clearly observed, the amounts of  $\text{U}^{\text{IV}}$  and  $\text{U}^{\text{V}}$  continuously decreasing and increasing, respectively, with potential. In carbonate-free solutions, the  $\text{U}^{\text{VI}}$  content of the surface also increases with increasing anodic potential. By contrast, in the carbonate solution, the  $\text{U}^{\text{VI}}$  content of the surface does not increase, consistent with the expectation that  $\text{U}^{\text{VI}}$  (as  $\text{U}^{\text{VI}}\text{O}_2(\text{CO}_3)_x^{(2-2x)+}$ ).

For the Gd- $\text{UO}_2$  electrode, for potentials  $\geq 0.2$  V in the presence of carbonate, the surface composition ( $\text{U}^{\text{IV}}/\text{U}^{\text{V}}$  ratio) becomes independent of potential which coincides with the range (0.2 V to 0.4 V) over which the steady-state currents become potential-independent, Fig. 6. This indicates that the surface  $\text{U}^{\text{IV}}_{1-2x}\text{U}^{\text{V}}_{2x}\text{O}_{2+x}$  layer has

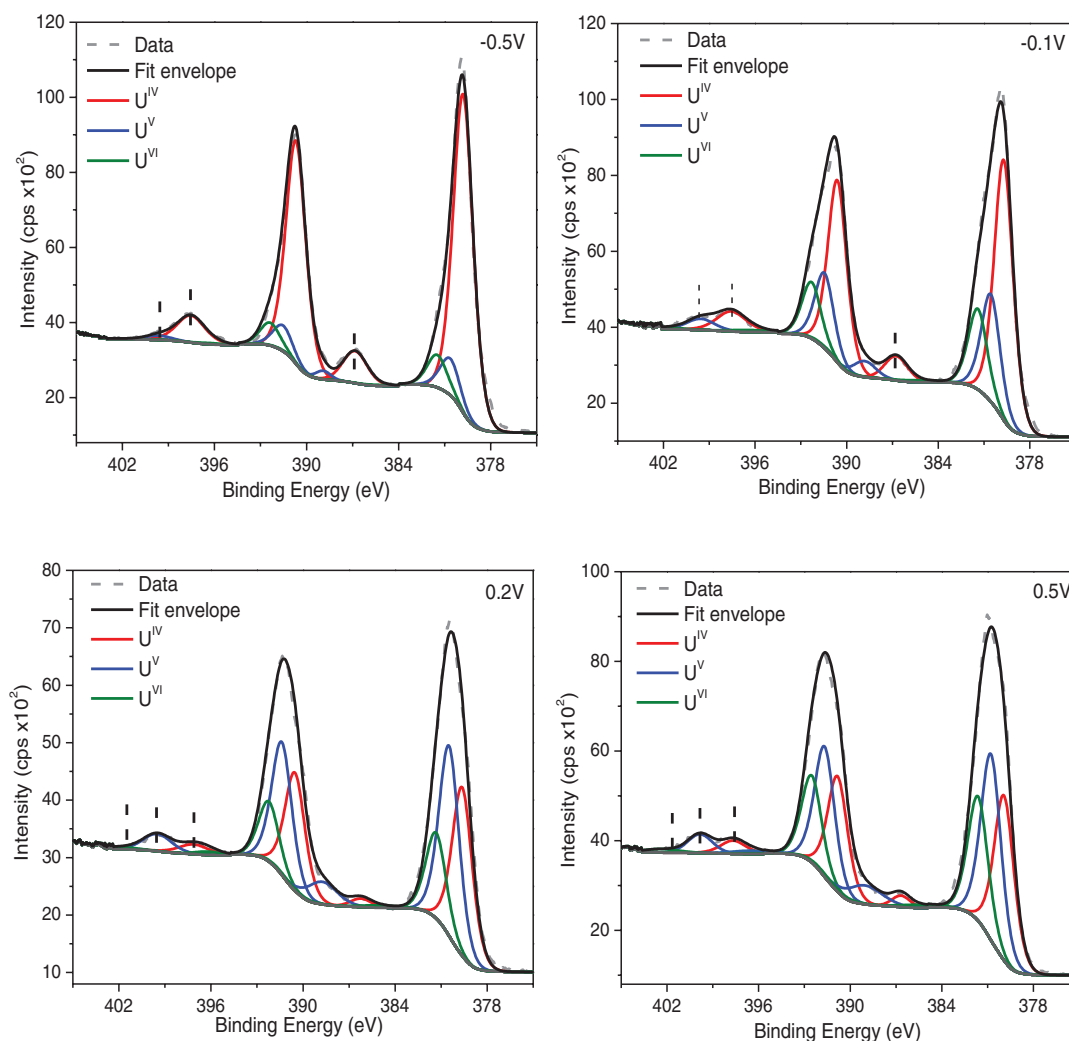


**Figure 7.** Representative U 4f XPS spectra resolved into contributions from  $\text{U}^{\text{IV}}$ ,  $\text{U}^{\text{V}}$  and  $\text{U}^{\text{VI}}$  recorded on a Gd-doped  $\text{UO}_2$  electrode in an Ar-purged  $0.1 \text{ mol.L}^{-1}$  NaCl solution, pH 9, at a series of applied potentials  $-0.5$ ,  $-0.1$ ,  $0$  and  $0.2$  V.

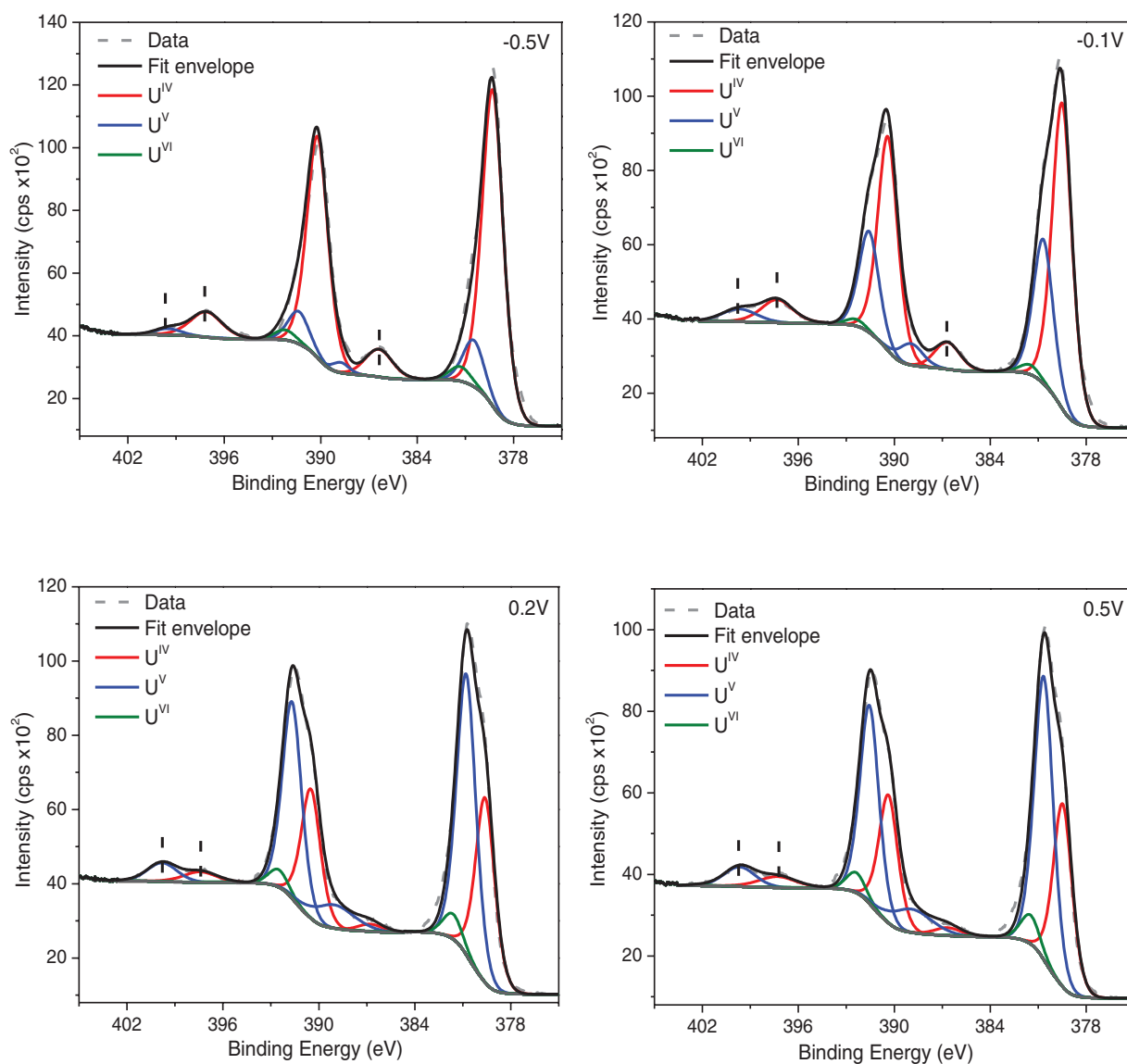


**Figure 8.** Representative U 4f XPS spectra resolved into contributions from  $U^{IV}$ ,  $U^V$  and  $U^{VI}$  recorded on a Gd-doped  $UO_2$  electrode in an Ar-purged 0.1 mol.  $L^{-1}$  NaCl solution, pH 9, containing  $[HCO_3^-/CO_3^{2-}] = 5 \times 10^{-2}$  mol. $L^{-1}$  at a series of applied potentials  $-0.5$ ,  $-0.1$ ,  $0$  and  $0.2$  V.

achieved compositional steady-state in the presence of carbonate. The absence of  $U^{VI}$  on the electrode surface over the full potential range indicates that any  $UO_2^{2+}$  species formed are chemically dissolved into solution as soon as they are electrochemically formed. In addition, the presence of a strong  $U^V$  signal is consistent with the voltammetric data (Fig. 4) which shows that the extent of oxidation of the surface, as illustrated by the constant height of the cathodic reduction peak, remains constant as the carbonate concentration is increased.

In the absence of carbonate, the  $U^V$  content of the surface also becomes effectively constant at high potentials, the changes in fractional composition occurring mainly between  $U^{IV}$  and  $U^{VI}$ . The retention of  $U^{VI}$  as a partially insulating surface layer would account for the considerably lower anodic currents observed, Fig. 6. The slight loss of  $U^{VI}$  at the most positive potentials (0.45 V and 0.5 V) is consistent with the enhanced anodic dissolution currents observed at these potentials, Fig. 6, attributable to local acidification at some locations on the electrode surface.

Figure 10 compares the influence of potential on the  $U^V$  content of the surface for Gd- $UO_2$  in both carbonate and non-carbonate containing solutions to that of SIMFUEL in the absence of car-

bonate. The higher  $U^V$  content on SIMFUEL in the potential range  $< -0.25$  V may reflect our improved procedure in avoiding air oxidation when the anodically oxidized electrode is transferred from the electrochemical cell to the spectrometer. Despite this apparent artifact it is clear that extensive oxidation of the surface, via the incorporation of  $O^{2-}$  interstitial ions and the creation of  $U^V$  states, begins in all cases around  $\sim -0.25$  V consistent with the current increases observed in CVs, Fig. 4. This observation confirms that the surface oxidation to  $U^{IV}_{1-2x}U^V_{2x}O_{2+x}$  is not noticeably delayed on the potential scale by RE<sup>III</sup>-doping at least up to the 6 wt% Gd used in the present studies.

The anodic currents measured at potentials in the vicinity of  $-0.25$  V are small and only marginally dependent on carbonate concentration, Figs. 4 and 5, indicating only marginal dissolution as  $U^{VI}$  is occurring. However, as shown previously in voltammetric experiments<sup>20</sup> the anodic currents measured on Gd- $UO_2$  are considerably lower than on SIMFUEL. This is confirmed by the larger  $U^V$  content, and its more rapid increase with potential, on the surface of the SIMFUEL compared to that of Gd- $UO_2$  (in the absence of carbonate), Fig. 10.

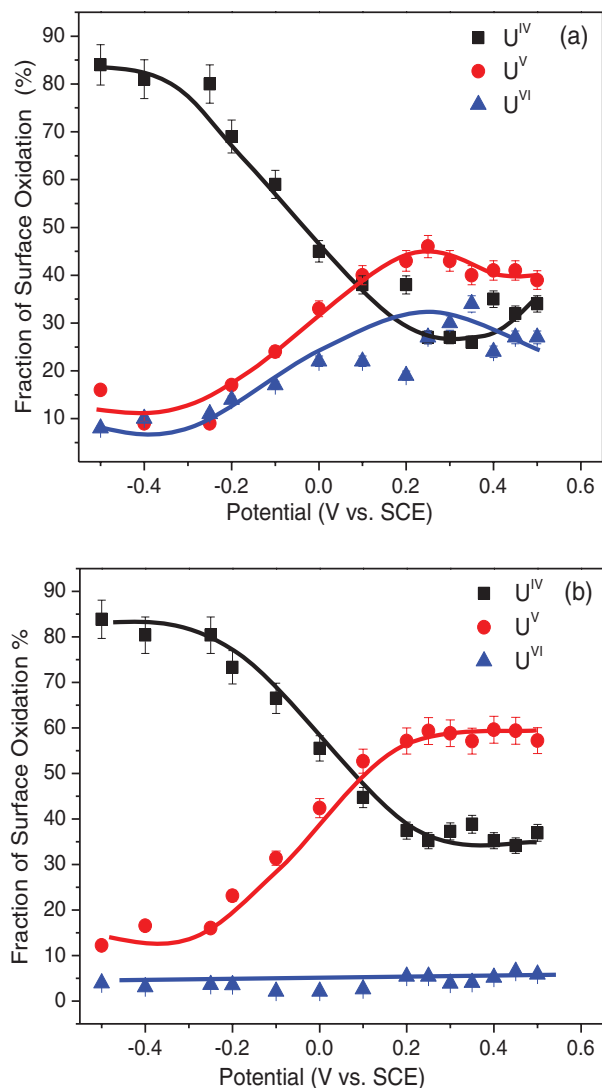


**Figure 9.** Relative fractions of all three U oxidation states as a function of applied potential (for 1 hour) in an Ar-purged 0.1 mol.L<sup>-1</sup> NaCl solution, pH 9, (a) without (from Fig. 7) and (b) with (from Fig. 8) carbonate ( $[HCO_3^-/CO_3^{2-}] = 5 \times 10^{-2}$  mol.L<sup>-1</sup>) in solution.

Previously, the ability of RE<sup>III</sup> doping to suppress anodic oxidation of the  $UO_2$  matrix (to  $U^{IV}_{1-2x}U^V_{2x}O_{2+x}$ ) has been attributed to the formation of RE<sup>III</sup>-O<sub>V</sub> clusters which limits the availability of the O<sub>V</sub> required for the incorporation of O<sup>2-</sup> ions as oxidation proceeds.<sup>20</sup> In addition, it was suggested that Gd-doping leads to a lattice contraction and a decreased mobility of O<sup>2-</sup> to deeper locations within the  $UO_2$  surface. This combination of unavailable O<sub>V</sub> and limited O<sup>2-</sup> mobility in the  $UO_2$  matrix would account for the lower  $U^V$  surface content and its slower increase with potential on Gd- $UO_2$  compared to SIMFUEL.

At more positive potentials, when the conversion of  $U^V$  to  $U^{VI}$  becomes important there is a considerable difference in the  $U^V$  contents. The very high content on the Gd- $UO_2$  surface when carbonate is present reflects a combination of the stability of the  $U^{IV}_{1-2x}U^V_{2x}O_{2+x}$  and the absence of  $U^{VI}$  rapidly chemically dissolved into solution as  $UO_2(CO_3)_x^{(2-2x)+}$ . Unfortunately, a similar set of XPS experiments on SIMFUEL in the presence of carbonate are presently unavailable. In the absence of carbonate, the  $U^V$  content begins to decrease at a much lower potential and decreases to considerably lower values at high potentials on SIMFUEL than on Gd- $UO_2$ , Fig. 10. This can be attributed to the oxidation step

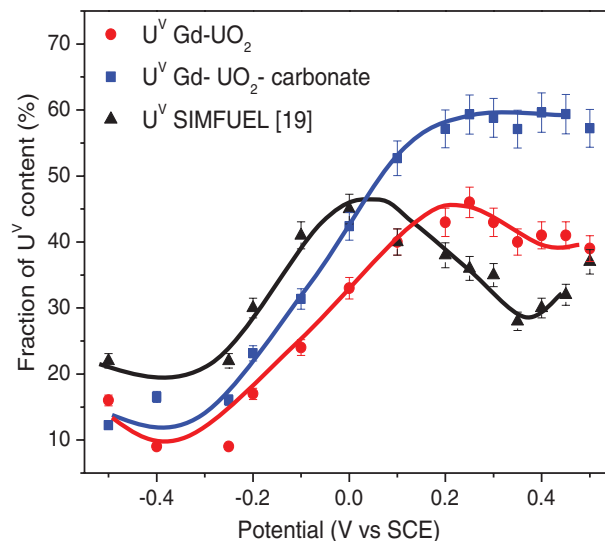


**Figure 10.** Fraction of  $U^V$  in the surface of Gd- $UO_2$  and SIMFUEL<sup>19</sup> as a function of applied potential after potentiostatic treatment (for 1 hour) in an Ar-purged 0.1 mol.L<sup>-1</sup> NaCl solution, pH 9, with and without carbonate.

and is consistent with the higher  $U^{VI}$  content on the SIMFUEL surface compared to the Gd- $UO_2$  surface, Fig. 9a. These results show that Gd-doping (to 6 wt%) inhibits both the kinetics of the matrix surface oxidation (to  $U^{IV}_{1-2x}U^V_{2x}O_{2+x}$ ) and especially its further oxidation (to  $UO_3 \cdot yH_2O$ ).

**Cathodic stripping voltammetry (CSV).**— Figure 11 shows a series of cathodic stripping voltammograms recorded after potentiostatic polarization for 1 hour at individual potentials in the range -0.5 V to 0.4 V; i.e., for the same potentials and times used in the potentiostatic experiments (Fig. 5) prior to XPS analyses (Fig. 9). Figure 11a shows the results recorded in a solution containing no carbonate and Fig. 11b the results recorded in a solution containing  $5 \times 10^{-2}$  mol.L<sup>-1</sup> of carbonate. The main reduction peak, centered in the potential range -0.6 V to -0.9 V has been previously observed on undoped  $UO_2$ <sup>4</sup> and SIMFUEL,<sup>18</sup> and attributed to the reduction of the anodically formed surface films.

In the absence of carbonate, Fig. 11a, there appear to be two reduction peaks in this region, possibly reflecting the dual phase nature of the surface film ( $U^{IV}_{1-2x}U^V_{2x}O_{2+x}/U^{VI}O_{3,y}H_2O$ ). In the presence of carbonate, Fig. 11b, the reduction peak at more negative potentials is not present. Since XPS shows no  $U^{VI}$  accumulates on the electrode surface when carbonate is present, Fig. 9b, it is possible this reduction process at more negative potentials can be attributed to the reduction of  $UO_3 \cdot yH_2O$  present on the electrode surface when carbonate is absent. This would then indicate the reduction at less negative potentials, observed irrespective of whether carbonate is present, can be attributed to the reduction of the oxidized matrix ( $U^{IV}_{1-2x}U^V_{2x}O_{2+x}$ ).

Figure 12 shows the total charge due to film reduction as a function of the applied potential, calculated by integrating the CSVs in Fig. 11 between the potential limits -1.2 V and 0.4 V. Two distinct regions of behavior are observed. Up to 0.1 V the charge is independent of whether carbonate is present or not, confirming that the matrix oxidation reaction does not involve carbonate. At more positive potentials the reduction charge increases in the absence of carbonate, consistent with the accumulation of  $U^{VI}$  (as  $U^{VI}O_{3,y}H_2O$ ) on the electrode surface (Fig. 9a) and the presence of a dual reduction peak in the CSV, Fig. 11a.

When carbonate is present the charge due to film reduction reaches a peak value around 0.1 V; i.e., the potential at which the composition reaches a plateau value (Fig. 9b). At more positive potentials the charge decreases slightly to a potential independent value. Since EDX analyses, Fig. 1b show the Gd is uniformly distributed within the

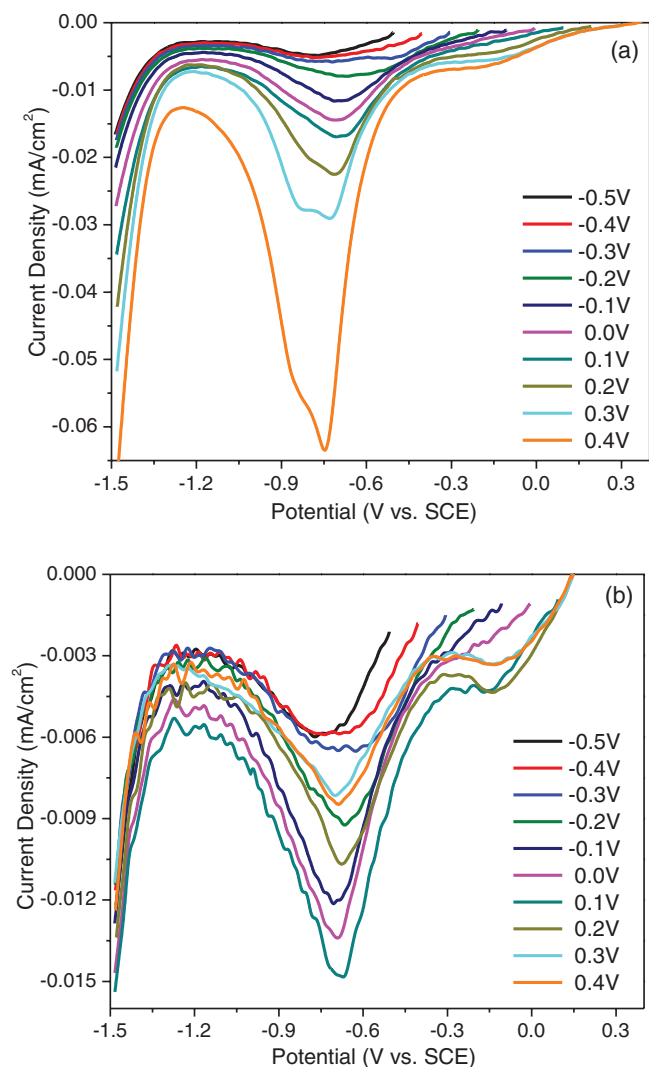


**Figure 11.** Cathodic stripping voltammograms (CSV) recorded on a Gd-doped  $\text{UO}_2$  electrode after potentiostatic treatments (for 1 hour) at various potentials in an Ar-purged  $0.1 \text{ mol.L}^{-1}$  NaCl solution, pH 9, (a) without and (b) with carbonate ( $[\text{HCO}_3^-/\text{CO}_3^{2-}] = 5 \times 10^{-2} \text{ mol.L}^{-1}$ ) at an electrode rotation rate of 16.67 Hz.

$\text{UO}_2$  matrix it is reasonable to assume that matrix oxidation is also uniform, and the charge can be taken as a measure of the thickness of the oxidized surface layer. Thus, when carbonate is present the  $\text{U}^{\text{IV}}_{1-2x}\text{U}^{\text{V}}_{2x}\text{O}_{2+x}$  surface layer achieves both a constant thickness and a constant composition. This combination and the absence of  $\text{U}^{\text{VI}}$  on the electrode surface indicates that the overall rate determining step in the anodic reaction is the creation of  $\text{U}^{\text{VI}}$  by oxidation of the  $\text{U}^{\text{IV}}_{1-2x}\text{U}^{\text{V}}_{2x}\text{O}_{2+x}$  surface layer.

This provides strong evidence that the dominant influence of Gd doping is the inhibition of reaction 4; i.e., the second stage of the oxidation/dissolution step. In this regard the influence of  $\text{RE}^{\text{III}}$  doping on the two stages of anodic oxidation/dissolution is very similar to its influence on the two stages of air oxidation.<sup>8,10,13,31</sup>

These results confirm that the influence of rare-earth doping of the  $\text{UO}_2$  matrix is to suppress its anodic reactivity. In this regard this influence is similar to that observed for the air oxidation of the fuel. Since the extent of  $\text{RE}^{\text{III}}$  doping will increase with in-reactor burn up (i.e., the fraction of  $^{235}\text{U}$  atoms consumed by fission) our results show that this aspect of the fission process will lead to a more stable fuel wastefrom less likely to release radionuclides within a failed waste container.

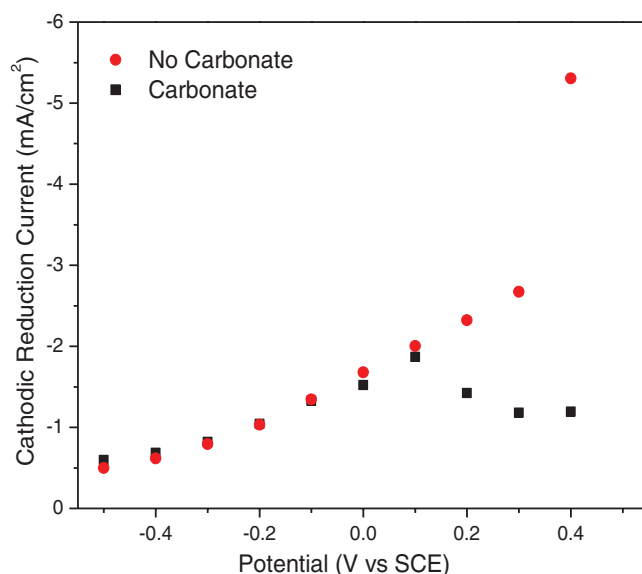


**Figure 12.** Total cathodic charge obtained by integration of the reduction peaks in the CSVs in Fig. 11.

## Conclusions

The effect of Gd doping (to 6 wt%) on the electrochemical behavior of  $\text{UO}_2$  has been investigated in neutral to slightly alkaline solutions with and without carbonate, and the results compared to similar experiments performed previously on 1.5 at% SIMFUEL.

The anodic oxidation/dissolution mechanism on Gd- $\text{UO}_2$  is similar to that observed on SIMFUEL although the overall reactivity of Gd- $\text{UO}_2$  is much lower.

Gd-doping inhibits the anodic oxidation of  $\text{UO}_2$ . This can be attributed to the presence of  $\text{Gd}^{\text{III}}\text{-O}_\text{V}$  clusters which reduces the availability of the  $\text{O}_\text{V}$  required to accommodate excess  $\text{O}^{2-}$  ions when oxidation occurs. Doping also leads to a lattice contraction which reduces the  $\text{O}^{2-}$  mobility in the  $\text{UO}_2$  matrix and limits oxidation to a thin surface layer of  $\text{U}^{\text{IV}}_{1-2x}\text{U}^{\text{V}}_{2x}\text{O}_{2+x}$ .

Gd-doping also hinders further oxidation of this thin layer to produce soluble  $\text{UO}_2^{2+}$ . In carbonate solutions any  $\text{UO}_2^{2+}$  formed is rapidly dissolved (as  $\text{U}^{\text{VI}}\text{O}_2(\text{CO}_3)_x^{(2-2x)+}$ ) and the rate determining step in the overall anodic matrix oxidation/dissolution process is the oxidation of the  $\text{U}^{\text{IV}}_{1-2x}\text{U}^{\text{V}}_{2x}\text{O}_{2+x}$  to produce  $\text{UO}_2^{2+}$ .

## Acknowledgment

This research was funded under the Canadian Natural Sciences and Engineering Research Council (NSERC) and Nuclear Waste Management Organization (NWMO), Toronto, Canada. Surface Science Western is greatly acknowledged for the use of their equipment.

## References

1. Nuclear Waste Management Organization (NWMO). *Choosing a Way Forward: The Future Management of Canada's Used Nuclear Fuel*. (Available at [www.nwmo.ca](http://www.nwmo.ca)) (2005).
2. J. McMurry, D. A. Dixon, J. D. Garroni, B. M. Ikeda, S. Stroes-Gascoyne, P. Baumgartner, and T. W. Melnyk, Ontario Power Generation Report No: 06819-REP-01200-10092-R00 (2003), Toronto, Ontario, Canada.
3. F. King and M. Kolar, Ontario Power Generation Report, 06819-REP-01200-10041-R00 (2000), Toronto, Ontario, Canada.
4. D. W. Shoesmith, *J. Nucl. Mater.*, **282**, 1 (2000).
5. H. He, M. Broczkowski, K. O'Neil, D. Ofori, O. Semenikhin, and D. W. Shoesmith, Nuclear Waste Management Organization, NWMO TR-2012-09 Toronto (2012).
6. R. J. McEachern, D. C. Doern, and D. D. Wood, *J. Nucl. Mater.*, **252**, 145 (1998).
7. R. D. Scheele, B. D. Hanson, S. E. Cumbledge, E. D. Jenson, A. E. Kozelisky, R. L. Sell, P. J. MacFarlan, and L. A. Snow, *Scientific Basis for Nuclear Waste Management XXVIII: Material Research Society Symposium Proceedings* (2004).
8. L. E. Thomas, R. E. Einziger, and H. C. Buchanan, *J. Nucl. Mater.*, **201**, 310 (1993).

9. R. J. McEachern, *J. Nucl. Mater.*, **245**, 238 (1997).
10. R. J. McEachern and P. Taylor, *J. Nucl. Mater.*, **254**, 87 (1998).
11. G. S. You, K. S. Kim, D. K. Min, and S. G. Ro, *J. Nucl. Mater.*, **277**, 325 (2000).
12. K. Ollila and K. Lindqvist, *Geological Survey of Finland, Oikiluoto*, Finland (2003).
13. B. D. Hanson, *Pacific Northwest National Laboratory 11929, Richland*, Washington (1998).
14. T. K. Campbell, E. R. Gilbert, G. D. White, G. F. Piepel, and B. Wrona, *Nucl. Tech.*, **85**, 160 (1989).
15. R. E. Einziger, L. E. Thomas, H. C. Buchanan, and R. B. Stout, *J. Nucl. Mater.*, **190**, 53 (1992).
16. L. E. Thomas, R. E. Einziger, and R. E. Woodley, *J. Nucl. Mater.*, **166**, 243 (1989).
17. S. Sunder and N. H. Miller, *J. Nucl. Mater.*, **231**, 121 (1996).
18. D. W. Shoesmith, Nuclear Waste Management Organization Report, TR-2007-03(2007), Toronto, Ontario, Canada.
19. B. G. Santos, H. W. Nesbitt, J. J. Noel, and D. W. Shoesmith, *Electrochim. Acta*, **49**, 1863 (2004).
20. M. Razdan and D. W. Shoesmith, *J. Electrochem. Soc.*, **161**, H105 (2014).
21. K. Park and D. R. Olander, *J. Nucl. Mater.*, **187**, 89 (1992).
22. L. Desgranges, Y. Pontillon, P. Matheron, M. Marcet, P. Simon, G. Guimbretiere, and F. Porcher, *Inorg. Chem.*, **51**, 9147 (2012).
23. I. Grenthe, J. Fuger, R. J. Konings, R. J. Lemire, A. B. Muller, C. Nguyen-Trung, and H. Wanner, *Chemical Thermodynamics of Uranium*, North Holland, Amsterdam (1992).
24. D. W. Shoesmith, S. Sunder, M. G. Bailey, G. J. Wallace, and F. W. Stanchell, *Appl. Surf. Sci.*, **20**, 39 (1984).
25. J. S. Goldik, H. W. Nesbitt, J. J. Noël, and D. W. Shoesmith, *Electrochim. Acta*, **49**, 1699 (2004).
26. M. Razdan, D. S. Hall, P. G. Keech, and D. W. Shoesmith, *Electrochim. Acta*, **83**, 410 (2012).
27. H. He, P. G. Keech, M. E. Broczkowski, J. J. Noel, and D. W. Shoesmith, *Can. J. Chem.*, **85**, 1 (2007).
28. D. Manara and B. Renker, *J. Nucl. Mater.*, **321**, 233 (2003).
29. L. Desgranges, G. Baldinozzi, P. Simon, G. Guimbretière, and A. Canizares, *J. Raman Spec.*, **43**, 455 (2012).
30. P. G. Keech, J. S. Goldik, Z. Qin, and D. W. Shoesmith, *Electrochim. Acta*, **56**, 7923 (2011).
31. J. G. Kim, Y. K. Ha, S. D. Park, K. Y. Jee, and W. H. Kim, *J. Nucl. Mater.*, **297**, 327 (2001).